

## Crystal structure of stage-1 iodine-intercalated superconducting $\text{IBi}_2\text{Sr}_2\text{CaCu}_2\text{O}_x$

N. Kijima and R. Gronsky

*National Center for Electron Microscopy, Materials Sciences Division, Lawrence Berkeley Laboratory, University of California, Berkeley, CA 94720, USA*

X.-D. Xiang, W.A. Vareka, A. Zettl, J.L. Corkill and Marvin L. Cohen

*Department of Physics, University of California, and Materials Sciences Division, Lawrence Berkeley Laboratory, Berkeley, CA 94720, USA*

Received 19 July 1991

The crystal structure of stage-1 iodine-intercalated superconducting  $\text{IBi}_2\text{Sr}_2\text{CaCu}_2\text{O}_x$  has been determined by transmission electron microscopy to belong to the superspace group  $C_{111}^{m2}$  with subcell lattice parameters  $a=5.4$  Å,  $b=5.4$  Å,  $c=18.9$  Å, and a structural modulation wavelength of 26 Å. Intercalated iodine atoms alter the atomic stacking across Bi–O layers from the staggered configuration characteristic of superconducting  $\text{Bi}_2\text{Sr}_2\text{CaCu}_2\text{O}_x$  to a vertically aligned configuration in  $\text{IBi}_2\text{Sr}_2\text{CaCu}_2\text{O}_x$ . From the atomic spacings apparent in the images, it is concluded that the iodine layers bond to their neighboring Bi–O layers by van der Waals interactions.

### 1. Introduction

Recently, a number of stage-1 iodine-intercalated  $\text{Bi}_2\text{Sr}_2\text{Ca}_{n-1}\text{Cu}_n\text{O}_x$  ( $n=1, 2, 3$ ) superconductors were discovered, and the superconducting response of these materials was related to the amount of lattice expansion induced along the  $c$ -axis [1,2] due to intercalation. Beginning with host superconductors  $\text{Bi}_2\text{Sr}_2\text{Ca}_{n-1}\text{Cu}_n\text{O}_x$  ( $n=1, 2, 3$ ), iodine was intercalated at temperatures in the range of 150–200°C for times between 10–15 days. Both the weight change and energy dispersive X-ray spectroscopy of the stage-1 iodine-intercalated materials yielded a 1:2 ratio of I to Bi, corresponding to the stoichiometric formula  $\text{IBi}_2\text{Sr}_2\text{Ca}_{n-1}\text{Cu}_n\text{O}_x$  ( $n=1, 2, 3$ ). X-ray diffraction analyses showed that iodine atoms intercalate between the Bi–O bilayers of all three compounds, with a corresponding expansion along the  $c$ -axis by about 3.6 Å for each Bi–O bilayer. The extinction rules in the powder X-ray diffraction patterns indicated that the intercalated iodine layers were epitaxial with respect to the adjacent Bi–O layers, but the staggered stacking of the basic building

blocks of the host materials was changed to a simpler stacking sequence in the intercalated materials, with a single basic block per new unit cell. It was also found from the temperature dependence of the AC and DC magnetic susceptibility that the stage-1 iodine-intercalated compounds behave as bulk superconductors with 2–10 K lower superconducting transition temperatures than those of the host materials.

The detailed crystal structures of these stage-1 iodine-intercalated superconductors have yet to be determined. Powder X-ray analysis alone is hindered by the alignment of the high-aspect-ratio platelets of the samples, yielding strong texture in the diffraction patterns, by a small amount of impurities in the host materials, and by the relatively weak intensities of diffraction peaks from host and intercalated materials, making it difficult to determine the exact position of iodine atoms in the  $a$ - $b$  plane. Another question of interest is the effect of iodine intercalation on the various modulated structures that have been observed [3] in the host materials, since the structural modulations are believed to be associated with the Bi–O bilayers which the iodine atoms in-

tercalate. In order to address these questions, a detailed study of the crystal structure of  $\text{IBi}_2\text{Sr}_2\text{CaCu}_2\text{O}_x$  has been undertaken using transmission electron microscopy.

## 2. Experimental

A single crystal of the iodine-intercalated superconductor  $\text{IBi}_2\text{Sr}_2\text{CaCu}_2\text{O}_x$  was prepared by encapsulating iodine and a high-quality single crystal of  $\text{Bi}_2\text{Sr}_2\text{CaCu}_2\text{O}_x$  in a Pyrex tube under a vacuum of  $<10^{-3}$  Torr. Iodine intercalation was carried out at  $150^\circ\text{C}$  for 10 days in a uniform-temperature furnace.

A transmission Laue pattern of the iodine-intercalated product was used to orient the crystal for precise cutting into thin wafers, which were subsequently sandwiched between silicon wafers, thinned, dimpled, and ion-milled to electron transparency. Ion milling was carried out at 77 K using argon ions accelerated at 3 kV and an incidence angle of 10 degrees. Transmission electron microscopy was performed in the Berkeley ARM-1000 operating at 800 kV. Images were Fourier filtered using the image processing program SEMPER [4], and compared with images simulated by the code NCEMSS [5] at the National Center for Electron Microscopy.

## 3. Results and discussion

Figure 1 shows selected area electron diffraction patterns of the iodine-intercalated compound in four different zone axes. Lattice parameters determined from direct measurements of these patterns are:  $a=5.4 \text{ \AA}$ ,  $b=5.4 \text{ \AA}$  and  $c=18.9 \text{ \AA}$ . The  $a$  and  $b$  axial lengths are identical to those of the host material, while the  $c$  parameter is  $3.6 \text{ \AA}$  longer than half of the  $c$  parameter in the host material. Primary reflections with indices  $h0l$  ( $h=2n+1$ ) shows extinctions, indicating that the candidate space groups for this crystal structure include  $\text{Pma}2$ ,  $\text{Pmam}$  (equivalent to  $\text{Pmma}$ ) and  $\text{P}2_1\text{am}$  (equivalent to  $\text{Pmc}2_1$ ).

Figure 2 shows a through-focus series of original high-resolution transmission electron micrographs (a, b, c), the corresponding processed images (d, e, f) and simulated images (g, h, i) with a  $[\bar{1}10]$  incident beam direction along the 7 nm thick sample.

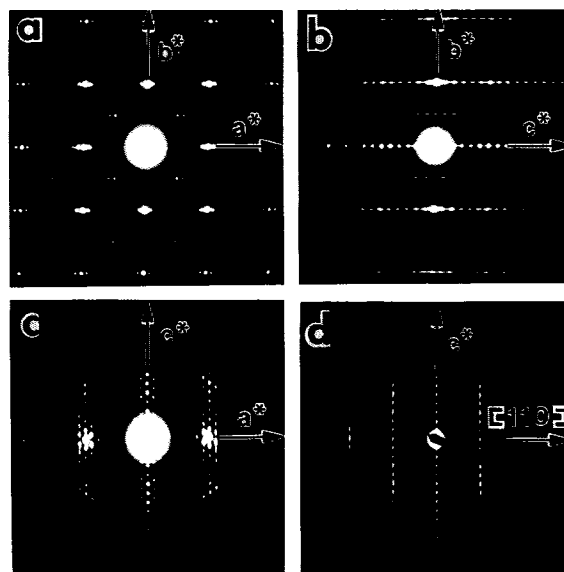


Fig. 1. Selected area electron diffraction patterns of the stage-1 iodine-intercalated superconductor  $\text{IBi}_2\text{Sr}_2\text{CaCu}_2\text{O}_x$ . (a)  $a^*-b^*$  plane, (b)  $b^*-c^*$  plane, (c)  $a^*-c^*$  plane, (d)  $[110]-c^*$  plane. The subcell lattice parameters are  $a=5.4 \text{ \AA}$ ,  $b=5.4 \text{ \AA}$  and  $c=18.9 \text{ \AA}$ . Primary reflections with indices  $h0l$  ( $h=2n+1$ ) show extinctions, indicating that the possible space groups for this crystal structure are  $\text{Pma}2$ ,  $\text{Pmam}$  (equivalent to  $\text{Pmma}$ ) and  $\text{P}2_1\text{am}$  (equivalent to  $\text{Pmc}2_1$ ).

Agreement is good for all three values of objective lens focus labeled in the left column ( $-14 \text{ nm}$ ,  $-22 \text{ nm}$ , and  $-30 \text{ nm}$ ). Figure 3 shows similar good agreement between the original image (a), processed image (b), and simulated image (c) of a 2.4 nm thick sample with its  $a$ -axis parallel to the incident electron beam, at  $-60 \text{ nm}$  underfocus. An enlargement of the processed image (fig. 3(b)) is shown in fig. 4, indicating the locations of the iodine atoms between Bi-O layers and an outline of the crystallographic unit cell. Table 1 summarizes the atomic positions within the intercalated crystal used during all image simulations in this study.

The dark dots corresponding to Bi atom positions marked "Bi" in fig. 4 line up in pairs because of the slight deviation of Bi atoms from their exact  $y=0.25$  positions (cf. fig. 8(c)). This deviation contributes to the excitation of diffraction spots with indices  $0kl$  where  $k=2n+1$  ( $n$  integer) as shown in fig. 1(b). A similar deviation of Bi positions has been reported for the host superconductor [6]. It is significant that

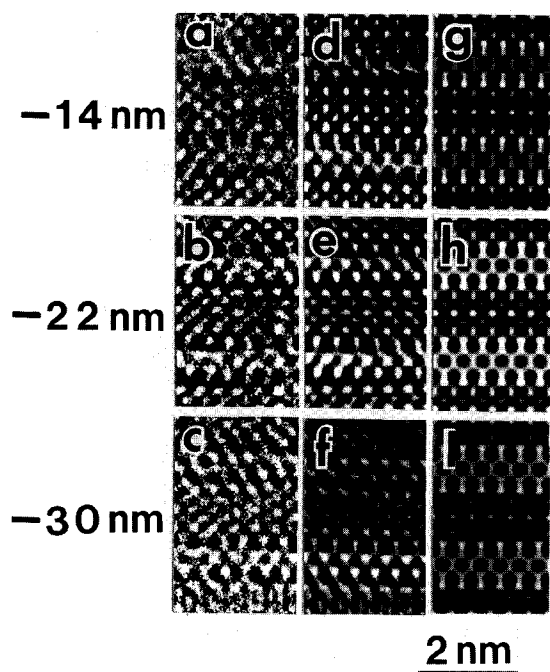


Fig. 2. Through-focus series with objective lens defoci  $-14\text{ nm} \sim -30\text{ nm}$ , of phase contrast high-resolution transmission electron microscope images (a)  $\sim$  (c), corresponding processed images (d)  $\sim$  (f) by means of Fourier filtering, and simulated images (g)  $\sim$  (i) using the atomic parameters in table 1. The incident electron beam is along the  $[110]$  direction. The specimen thickness is  $7\text{ nm}$ .

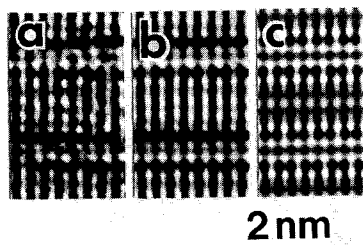


Fig. 3. Phase contrast high-resolution electron microscope image (a), corresponding processed image (b), and simulated image (c) of the stage-1 iodine-intercalated superconductor  $1\text{Bi}_2\text{Sr}_2\text{CaCu}_2\text{O}_x$  with an objective lens defocus  $-60\text{ nm}$ , and the incident electron beam along the  $a$ -axis. The specimen thickness is  $2.4\text{ nm}$ .

iodine intercalation does not change this structural feature in spite of a large expansion of the lattice along the  $c$ -axis. Every other Bi atom along the  $b$ -axis

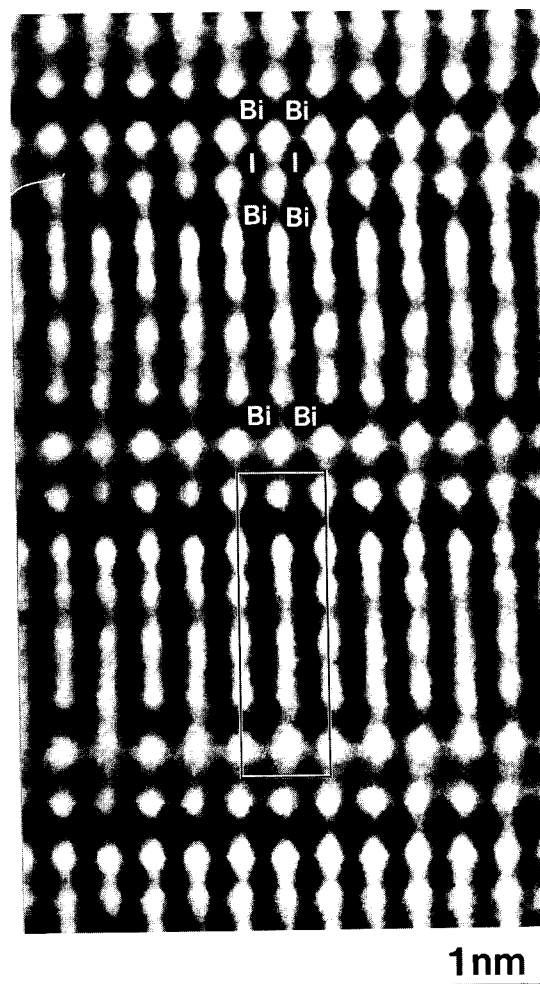


Fig. 4. Magnified version of the processed image of the stage-1 iodine-intercalated superconductor  $1\text{Bi}_2\text{Sr}_2\text{CaCu}_2\text{O}_x$  (fig. 3(b)) with the incident electron beam along the  $a$ -axis. Note that dark dots corresponding to Bi atom positions line up in pairs. The box shows the unit cell, which includes an iodine layer and a basic building block of Bi, Sr, Cu, Ca and oxygen atoms. Compare with fig. 8(c).

is located at  $x=0.25$ , while the others are located at  $x=0.75$ . Since no equivalent Bi atoms are observed along the  $a$ -axis in the high-resolution electron micrographs at positions yielded by the symmetry operation  $2_1$ , the candidate space groups  $\text{Pm}am$  and  $\text{P}2_1am$  have to be discarded, leaving  $\text{P}ma2$  as the only space group that corresponds both to the extinction rules observed in fig. 1 and to the symmetry oper-

Table 1  
Atomic positions for the iodine-intercalated superconductor  $\text{IBi}_2\text{Sr}_2\text{CaCu}_2\text{O}_x$  used in image simulations

Atom	Site	$x$	$y$	$z$
I	$2c$	0.25	0.75	0.0
Bi1	$2c$	0.25	0.22	0.175
Bi2	$2c$	0.25	0.28	0.825
Sr1	$2c$	0.25	0.75	0.323
Sr2	$2c$	0.25	0.75	0.677
Cu1	$2c$	0.25	0.25	0.413
Cu2	$2c$	0.25	0.25	0.587
Ca	$2c$	0.25	0.75	0.500
O1	$2c$	0.25	0.72	0.175
O2	$2c$	0.25	0.78	0.825
O3	$2c$	0.25	0.25	0.284
O4	$2c$	0.25	0.25	0.716
O5	$2a$	0.0	0.0	0.413
O6	$2b$	0.0	0.5	0.413
O7	$2a$	0.0	0.0	0.587
O8	$2b$	0.0	0.5	0.587

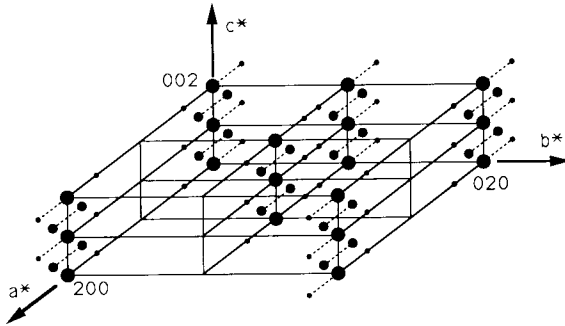


Fig. 5. Reciprocal lattice showing both the primary reflections and the satellite reflections based upon the selected area electron diffraction patterns in fig. 1. The allowed satellites have indices  $HKLm$  ( $L+m=2n$ ) and  $HOLm$  ( $H=2n$ ) where  $H=h$ ,  $K=k$ ,  $L=2l+m$ . This corresponds to the superspace group  $C_{111}^{Pma^2}$ , which is identical to the  $B_{111}^{Pc_2^m}$ . The  $a$ -axis component of a wave vector of the modulated structure is  $26 \text{ \AA}$ .

ations evident the images of figs. 2, 3 and 4. The image simulation was therefore carried out using the space group  $Pma2$ .

Satellite reflections are recorded in the diffraction pattern fig. 1(a) and (c), and are illustrated schematically in fig. 5. All satellite reflections can be related to the primary reflections by a vector with an irrational component along the  $a^*$ -axis and a rational component along the  $c^*$ -axis. The  $a$ -axis component of the modulation indicated by the satellite

reflections has a wavelength of  $26 \text{ \AA}$ , while the  $c$ -axis component has a wavelength of twice the  $c$  lattice parameter. Assigning four indices  $H$ ,  $K$ ,  $L$ , and  $m$  to the satellites in accordance with the procedure described by de Wolff et al. [7], it is found that the allowed satellites have indices  $HKLm$  ( $L+m=2n$ ) and  $HOLm$  ( $H=2n$ ) where  $H=h$ ,  $K=k$ ,  $L=2l+m$ . This corresponds to the superspace group  $C_{111}^{Pma^2}$ , which is identical to the  $B_{111}^{Pc_2^m}$ . Figure 6 is a high-resolution transmission electron micrograph of the iodine-intercalated compound with its  $b$ -axis parallel to the incident electron beam as shown in its corresponding electron diffraction pattern (inset). A “unit cell” of the regular lattice modulations is outlined, with regions of excess Bi atoms at its corners and at the cell center, and with a cell parameter of approximately  $5a$  by  $2c$ . This modulated structure is similar to that observed in the host superconductor  $\text{Bi}_2\text{Sr}_2\text{CaCu}_2\text{O}_x$ . Since intercalated iodine has little effect on the modulated structure in spite of its large atomic radius, it is most probable that the bonding between the iodine layer and the Bi–O bilayers is

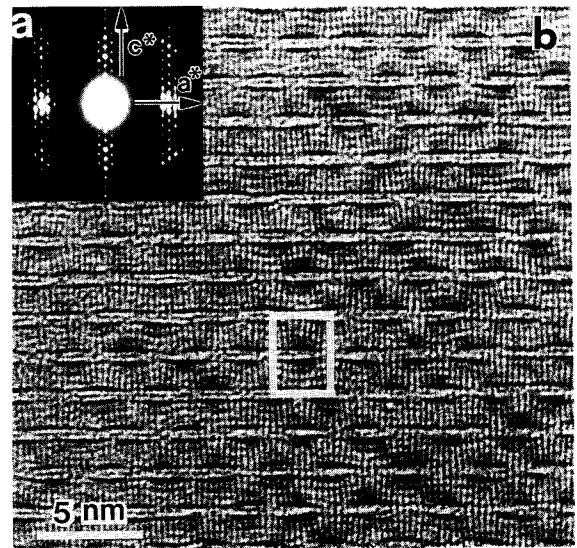


Fig. 6. Phase contrast high-resolution transmission electron microscope image (b) and corresponding selected area electron diffraction pattern (a) of the stage-1 iodine-intercalated superconductor  $\text{IBi}_2\text{Sr}_2\text{CaCu}_2\text{O}_x$  with the incident electron beam along the  $b$ -axis. A modulated structure with the  $a$ -axis component of a wave vector of  $26 \text{ \AA}$  is apparent, and highlighted by the box showing a minimum repeat unit for the modulated structure.

weak enough to have no effect on the bonds formed within the adjacent Bi–O layers.

The modulated structure of  $\text{Bi}_2\text{Sr}_2\text{CaCu}_2\text{O}_x$  was determined by a simultaneous refinement method using X-ray and TOF neutron diffraction data [8]. All of the atoms in the structure were found to be displaced from their average positions, with the oxygen atoms in the Bi–O layers undergoing the largest displacement. Although some displacement of atoms is evident in fig. 6, it is impossible to determine the actual atomic coordinates of the oxygen atoms in the Bi–O layers because of their smaller electron scattering coefficients relative to those of the adjacent heavy atoms. Therefore, the atomic coordinates of those oxygen atoms were fixed at the center of the adjacent four Bi atoms in the image simulations used in the present study.

Figure 7 shows the crystal structure of the stage-1 iodine-intercalated superconductor  $1\text{Bi}_2\text{Sr}_2\text{CaCu}_2\text{O}_x$ , while fig. 8 compares the structure of the stage-1 iodine-intercalated crystal with that of pristine  $\text{Bi}_2\text{Sr}_2\text{CaCu}_2\text{O}_x$ . The intercalated superconductor has

the same basic building blocks of Bi, Sr, Cu, Ca and oxygen as the host crystal, with one Ca layer, two Cu–O layers and two Sr–O layers sandwiched between double Bi–O layers. Following intercalation, iodine atoms are inserted between the Bi–O bilayers, and the effect on the surrounding lattice is most visible in images viewed along a  $[\bar{1}10]$  incident beam direction. In the host crystal, the basic building blocks are staggered by half of the  $b$  axial length (fig. 8(b)), while in the intercalated crystal, they are not (fig. 8(d)).

The actual location of iodine atoms in the Bi–O bilayer is apparent when comparing figs. 8(c), (d) and (f), which show that the iodine atoms are surrounded by two or four neighboring oxygen atoms, depending upon the phase of the structural modulation in which they reside. In fact, the relative positions of adjacent Bi atoms in the stage-1 iodine-intercalated superconductor is the same as those of the Bi atoms in the host crystal. It is therefore possible to model iodine intercalation as the simple substitution for I for Bi atoms in one of the Bi–O layers, resulting in the shift of the outwardly displaced Bi atoms by half of the  $b$  axial length, so that the Bi atoms in the upper (displaced) Bi–O layer occupy lattice sites equivalent to Bi atoms in the lower basic building block. This structural rearrangement results in a halving of the  $c$  axial length of  $1\text{Bi}_2\text{Sr}_2\text{CaCu}_2\text{O}_x$  relative to  $\text{Bi}_2\text{Sr}_2\text{CaCu}_2\text{O}_x$ . Table 2 is the comparison of the distances between adjacent cation layers in the stage-1 iodine-intercalated superconductor and the host superconductor, which shows that the expansion of the crystal along the  $c$ -axis by  $3.6 \text{ \AA}$  is associated with the  $3.4 \text{ \AA}$  expansion of the distance between the two Bi–O layers and the  $0.1 \text{ \AA}$  expansion between each Bi–Sr layer with an accuracy of 5% on atomic coordinates.

If there were no displacement of the oxygen atoms in the Bi–O layer relative to the center of the adjacent four Bi atoms, the interatomic distance between the iodine atoms and the oxygen atoms in the Bi–O layer would remain  $3.3 \text{ \AA}$ . However, since there is a modulation along the  $a$ -axis in the stage-1 iodine-intercalated crystal, this interatomic distance depends upon location within the modulation along the  $a$ -axis. Analysis of the modulated structure of the host  $\text{Bi}_2\text{Sr}_2\text{CaCu}_2\text{O}_x$  crystal, has shown that extra oxygen atoms are located in regions of excess Bi atoms where

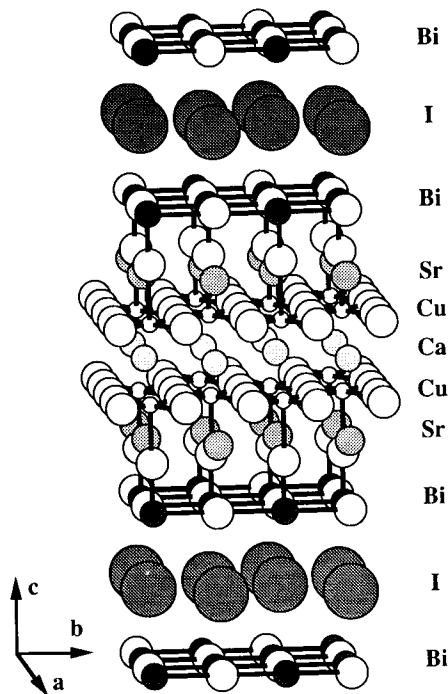


Fig. 7. Crystal structure of the stage-1 iodine-intercalated superconductor  $1\text{Bi}_2\text{Sr}_2\text{CaCu}_2\text{O}_x$ .

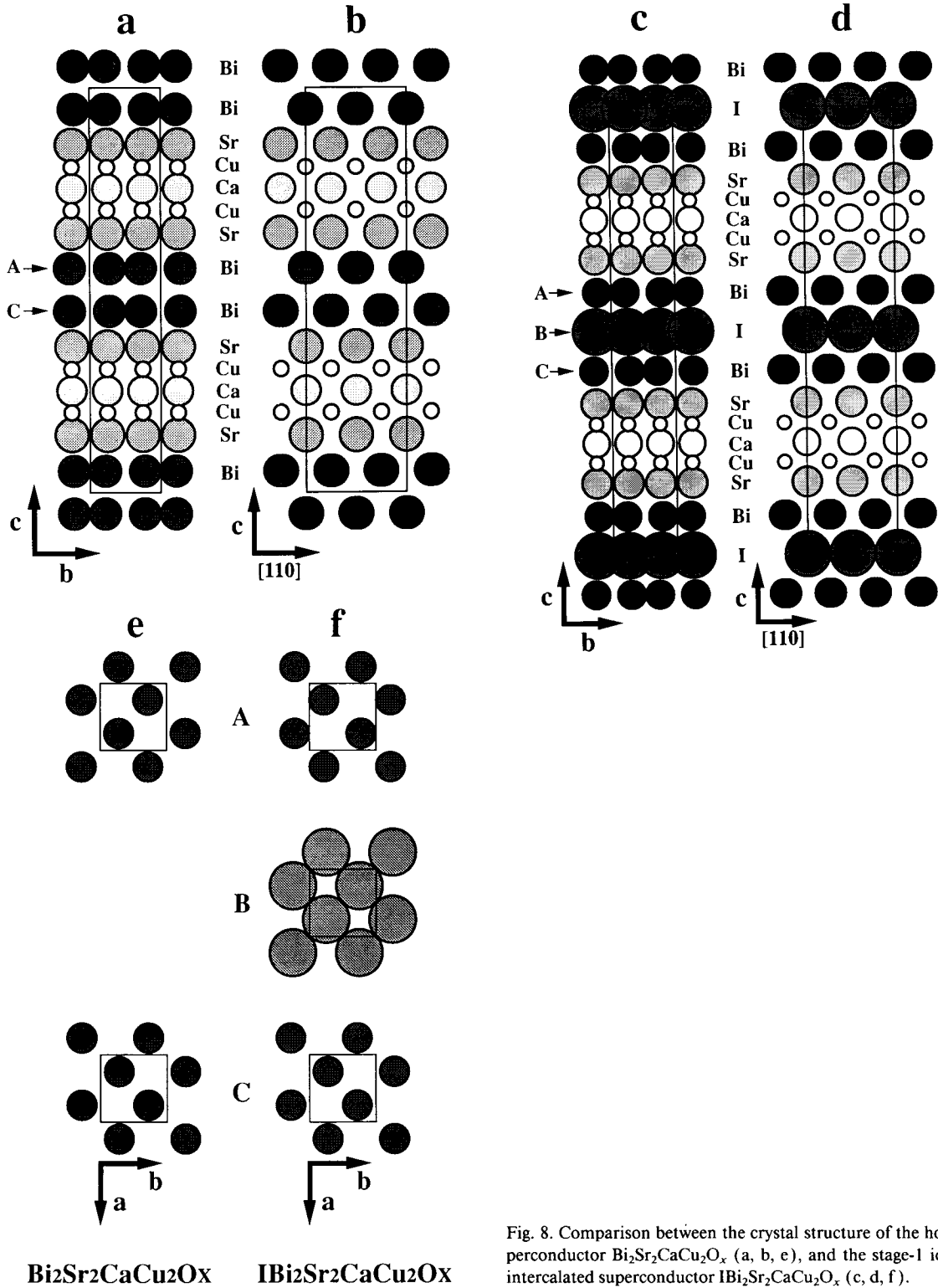


Fig. 8. Comparison between the crystal structure of the host superconductor  $Bi_2Sr_2CaCu_2O_x$  (a, b, e), and the stage-1 iodine-intercalated superconductor  $IBi_2Sr_2CaCu_2O_x$  (c, d, f).

Table 2

Comparison of the distances ( $\text{\AA}$ ) between adjacent cation layers in the iodine-intercalated superconductor  $\text{IBi}_2\text{Sr}_2\text{CaCu}_2\text{O}_x$  and the host superconductor  $\text{Bi}_2\text{Sr}_2\text{CaCu}_2\text{O}_x$ . The distances between the layers are defined using the  $z$  coordinates of the cations

Layers	$\text{IBi}_2\text{Sr}_2\text{CaCu}_2\text{O}_x$	$\text{Bi}_2\text{Sr}_2\text{CaCu}_2\text{O}_x$ <sup>a)</sup>
I-Bi	3.31	—
Bi-(1)-Bi	6.62	3.24
Bi-Sr	2.80	2.70
Sr-Cu	1.70	1.70
Cu-Ca	1.65	1.65

<sup>a)</sup> Ref. [8].

the distance between adjacent Bi-O layers is shorter than that in regions of dilute Bi [8]. Since a similar modulated structure is observed in the stage-1 iodine-intercalated crystal as shown in fig. 6, and since the intercalated iodine atoms uniformly expand the two Bi-O layers by an average of 3.4  $\text{\AA}$ , it is reasonable to infer that:

(1) in regions of excess Bi, the Bi-O layer spacing is 3.2  $\text{\AA}$ , with each iodine atom surrounded by four oxygens; and

(2) in regions of dilute Bi, the Bi-O layer spacing is 3.6  $\text{\AA}$ , with each iodine atom surrounded by two oxygens. These distances are much greater than expected for a covalent iodine-oxygen bond (the oxygen covalent radius is 0.66  $\text{\AA}$  and the iodine covalent radius is 1.33  $\text{\AA}$ ), and given the oxygen environment, an iodine anion (ionic radius 2.16  $\text{\AA}$ ) can also be ruled out. However, the summation of the van der Waals radii of iodine and oxygen is 3.55  $\text{\AA}$ , which is a much better fit to the average interatomic distances between the iodine layer and the Bi-O bilayer. Add to this the fact that  $\text{IBi}_2\text{Sr}_2\text{CaCu}_2\text{O}_x$  cleaves similarly along  $a$ - $b$  planes as  $\text{Bi}_2\text{Sr}_2\text{CaCu}_2\text{O}_x$ , and a prevailing van der Waals interaction between iodine layers and Bi-O layers is supported. Within the iodine layers, some covalent bonding is expected, and the observed interatomic half-separation of the planar face-centered array labeled B in fig. 8(f) is 1.9  $\text{\AA}$ , smaller than the iodine van der Waals radius of 2.15  $\text{\AA}$ .

According to the prevailing models of the Cu-based oxide superconductors [9], only the Cu-O planes are critical structural components in superconductivity; the other structural components appear to act as charge reservoirs which control the local charge

concentration within the Cu-O planes, and the superconducting transition temperature is closely related to the effective valence of the Cu atoms in the plane. In  $\text{IBi}_2\text{Sr}_2\text{CaCu}_2\text{O}_x$ , the intercalated iodine atoms obviously have no such effect on the transition temperature. It might be argued that if the intercalated iodine could have extracted electrons from the Bi-O layer, the resulting increase in holes within the Cu-O bands might have increased the carrier concentration and  $T_c$ . Unfortunately, the van der Waals interaction between iodine layers and adjacent Bi-O layers cannot bring about the necessary change in valence to increase  $T_c$ .

#### Acknowledgements

The Atomic Resolution Microscope, image analysis facilities, and technical support at the National Center for Electron Microscopy are gratefully acknowledged. This research is supported by the Director, Office of Energy Research, Office of Basic Energy Sciences, Materials Sciences Division, of the U.S. Department of Energy under Contract No. DE-AC03-76SF00098. JLC and MLC are supported by Natural Science Foundation Grant No. DMR88-18404. JLC acknowledges support from AT&T Bell Laboratories.

#### References

- [1] X.-D. Xiang, S. McKernan, W.A. Vareka, A. Zettl, J.L. Corkill, T.W. Barbee III and Marvin L. Cohen, *Nature* 348 (1990) 145.
- [2] X.-D. Xiang, A. Zettl, W.A. Vareka, J.L. Corkill, T.W. Barbee III and Marvin L. Cohen, *Phys. Rev. B* 43 (1991) 11496.
- [3] Y. Matsui and S. Horiuchi, *Jpn. J. Appl. Phys.* 27 (1988) L2306.
- [4] W.O. Saxton, T.J. Pitt and M. Horner, *Ultramicroscopy* 4 (1979) 343.
- [5] R. Kilaas, in: *Proc. of the 45th Annual Meeting of the Electron Microscopy Society of America*, ed. G.W. Bailey, Baltimore, Md. (1987) 66.
- [6] O. Eibl, *Physica C* 168 (1990) 215.
- [7] P.M. de Wolff, T. Janssen and A. Janner, *Acta Crystallogr. A* 37 (1981) 625.
- [8] A. Yamamoto, M. Onoda, E. Takayama-Muromachi, F. Izumi, T. Ishigaki and H. Asano, *Phys. Rev. B* 42 (1990) 4228.
- [9] R.J. Cava, *Science* 247 (1990) 656.